



New pyrimidine derivatives as efficient organic inhibitors on mild steel corrosion in acidic medium: Electrochemical, SEM, EDX, AFM and DFT studies



M. Yadav^{a,*}, S. Kumar^a, R.R. Sinha^a, I. Bahadur^{b,c,**}, E.E. Ebenso^{b,c}

^a Department of Applied Chemistry, Indian School of Mines, Dhanbad 826004, India

^b Material Science Innovation & Modelling (MaSIM) Research Focus Area, Faculty of Agriculture, Science and Technology, North-West University (Mafikeng Campus), Private Bag X2046, Mmabatho 2735, South Africa

^c Department of Chemistry, North-West University (Mafikeng Campus), Private Bag X2046, Mmabatho 2735, South Africa

ARTICLE INFO

Article history:

Received 18 February 2015

Received in revised form 23 June 2015

Accepted 25 June 2015

Available online xxxx

Keywords:

Mild steel
Pyrimidine derivatives
EIS
Polarization
Corrosion inhibition
DFT

ABSTRACT

New pyrimidine derivatives, namely, 7-methoxyprido [2,3-*d*]pyrimidin-4-amine (MPPA) and 4-amino-7-methoxyprido[2,3-*d*]pyrimidin-2(1*H*)-one (AMPO) were synthesized and their inhibitive action against the corrosion of mild steel in 15% HCl solution was studied by weight loss, potentiodynamic polarization and electrochemical impedance spectroscopy (EIS) techniques. Polarization studies showed that both studied inhibitors were of mixed type in nature. The adsorption of inhibitors on the mild steel surface obeys Langmuir adsorption isotherm. Scanning electron microscopy (SEM), energy dispersive X-ray spectroscopy (EDX) and atomic force microscopy (AFM) were performed for surface study of uninhibited and inhibited mild steel samples. Density functional theory (DFT) was employed for theoretical calculations.

© 2015 Elsevier B.V. All rights reserved.

1. Introduction

Acid solutions are commonly used for pickling, industrial acid cleaning, acid descaling, and oil-well acidifying [1–5] processes. In acidizing process of petroleum oil wells 15% of hydrochloric acid is forced into the well through steel tubing to open up near-bore channels in the formation and, hence, to increase the flow of oil. Because of the aggressiveness of acid solutions, mild steel corrodes severely during these processes, particularly with the use of hydrochloric acid, which results in terrible waste of both resources and money [6]. A corrosion inhibitor is often added to mitigate the corrosion of metal by acid attack. Most well-known corrosion inhibitors are organic compounds containing polar groups including nitrogen, sulfur, and/or oxygen atoms and heterocyclic compounds with polar functional groups and conjugated double bonds [7–13]. These compounds can adsorb on the metal surface and block the active sites on the surface, thereby reducing the corrosion rate. The pyrido[2,3-*d*]pyrimidine derivatives are of great interest in

organic chemistry, because manifold implications viz, antibacterial, antifungal, anticancer, antitumor, antiherpes, antiallergic, analgesic, anti-inflammatory, and antineoplastic are well proved by a large number of publication on it [14–16]. Due to presence of heteroatoms and delocalized π -electrons, some pyrimidine derivatives are also reported as good corrosion inhibitors [17–19].

In continuation of our research for developing corrosion inhibitors [20–27] with high effectiveness and efficiency, the present paper explores a systematic study to ascertain the inhibitive action of synthesized pyrimidine derivatives, namely, 7-methoxyprido[2,3-*d*]pyrimidin-4-amine (MPPA) and 4-amino-7-methoxyprido[2,3-*d*]pyrimidin-2(1*H*)-one (AMPO) on corrosion of mild steel in 15% HCl solution by using weight loss measurement, potentiodynamic polarization, AC impedance and quantum chemical calculations.

2. Experimental

2.1. Materials

2.1.1. Mild steel sample

Corrosion inhibition studies were performed on mild steel having the composition (wt.%): C, 0.12; Mn, 0.11; Cu, 0.01; Si, 0.02; Sn, 0.01; P, 0.02; Ni, 0.02 and balance Fe. Mild steel samples used in the weight loss experiment were mechanically cut into 3.0 cm × 3.0 cm × 0.1 cm

* Corresponding author.

** Correspondence to: I. Bahadur, Material Science Innovation & Modelling (MaSIM) Research Focus Area, Faculty of Agriculture, Science and Technology, North-West University (Mafikeng Campus), Private Bag X2046, Mmabatho 2735, South Africa.

E-mail addresses: yadavdrmahendra@yahoo.co.in (M. Yadav), bahadur.indra@gmail.com (I. Bahadur).

dimensions, abraded with SiC abrasive papers of grade 320, 400 and 600 respectively. For potentiodynamic polarization and AC impedance studies, mild steel samples having dimension $1.0 \text{ cm} \times 1.0 \text{ cm} \times 0.1 \text{ cm}$ were mechanically cut and abraded similarly to a previous procedure, with an exposed area of 1 cm^2 (the rest covered with araldite resin) with 3 cm long stem. Before starting the experiment, mild steel samples were washed with distilled water, degreased in acetone, dried and stored in vacuum desiccator.

2.1.2. Test solution

The test solutions (15% HCl solution) were prepared by dilution of analytical grade 37% HCl with distilled water. The concentration range of inhibitors was 50–200 ppm (mg L^{-1}) and the volumes of test solution used for weight loss measurement and electrochemical studies were 250 mL and 150 mL, respectively.

2.1.3. Synthesis of corrosion inhibitors

The inhibitors MPPA and AMPO were synthesized by the method reported in literature [28]. Chalcone was synthesized by stirring a mixture of benzaldehyde (0.1 mol), 4-methoxyacetophenone (0.1 mol) and small amount of sodium hydroxide in ethanol (50 mL). A mixture of the chalcone (0.05 mol), malononitrile (0.05 mol) and ammonium acetate (0.4 mol) in ethanol (80 mL) was refluxed on a water bath for 14–16 h to synthesize 2-amino-3-cyano-6-methoxypyridine. The

compounds MPPA and AMPO were obtained by refluxing a mixture of 2-amino-3-cyano-6-methoxypyridine (0.04 mol) with formamide (0.04 mol) and urea (0.04 mol) respectively, on an oil bath. The synthetic route of inhibitors (MPPA and AMPO) is shown in Scheme 1 and the structure of inhibitors is shown in Fig. 1. The purity of the inhibitors was checked by thin layer chromatography (TLC). The IR and ^1H NMR spectra of inhibitors MPPA and AMPO are given in supplementary materials as Figs. S1 and S2, respectively. The melting point, yield, IR, ^1H NMR and ^{13}C data of the synthesized compounds are given below:

MPPA

Yield (74%), m.p. = 107–109 °C. Anal.: Calculated for $\text{C}_8\text{H}_8\text{N}_4\text{O}$; C, 54.54; H, 4.58; N, 31.80;

Found: C, 54.51; H, 4.57; N, 31.79

IR (ν/cm^{-1}): 3260 (NH), 1665 (C=N), 2940 (CH alkyl)

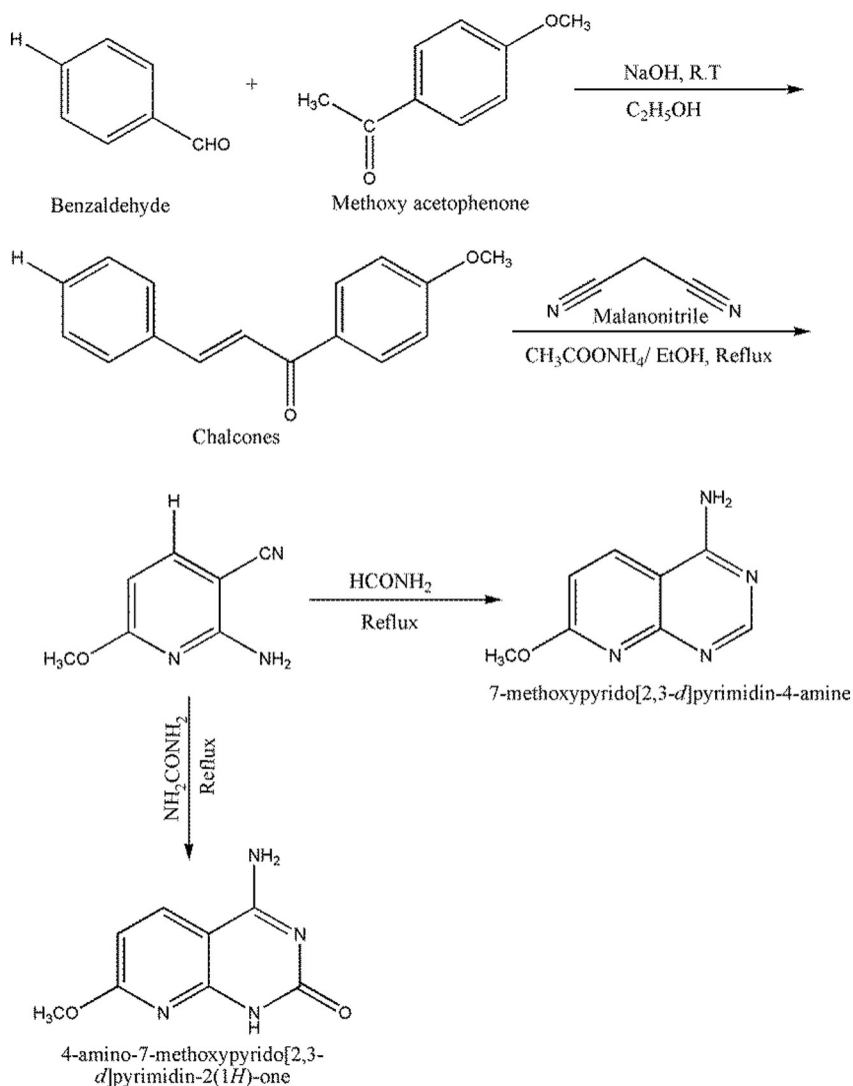
^1H NMR (300 MHz, $\text{DMSO-}d_6$) δ ppm: 7.72 (s, 2H, $-\text{NH}_2$), 3.7 (s, 3H, $-\text{OCH}_3$), 6.52 (m, 2H, pyridine), 8.24 (m, H, pyrimidine)

^{13}C NMR (300 MHz, CDCl_3) δ ppm: 164.8, 161.6, 156.4, 150.2, 142.3, 114.6, 59.6.

AMPO

Yield (76%), m.p. = 115–118 °C. Anal.: Calculated for $\text{C}_8\text{H}_8\text{N}_4\text{O}_2$; C, 50.00; H, 4.20; N, 29.15.

Found: C, 49.97; H, 4.19; N, 29.14



Scheme 1. Synthetic route of inhibitors 7-methoxyprido[2,3-d]pyrimidin-4-amine (MPPA) and 4-amino-7-methoxyprido[2,3-d]pyrimidin-2(1H)-one (AMPO).

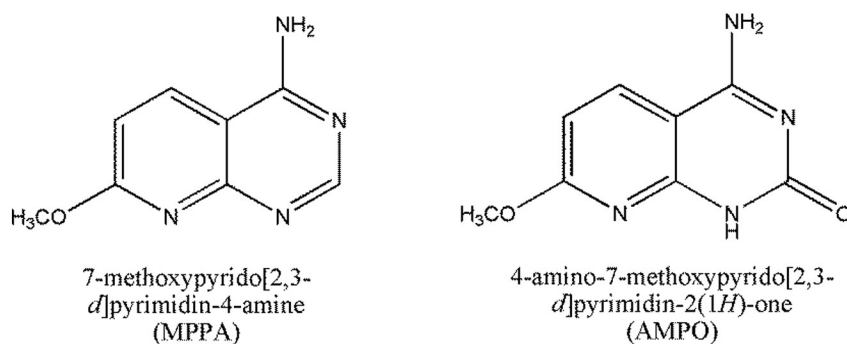


Fig. 1. Structure of inhibitors 7-methoxypyrido[2, 3-d]pyrimidin-4-amine (MPPA) and 4-amino-7-methoxypyrido[2, 3-d]pyrimidin-2(1H)-one (AMPO).

IR (ν/cm^{-1}): 3250 (NH), 1660 (C=N), 1720 (C=O), 2920 (CH alkyl)
¹H NMR (300 MHz, DMSO-*d*₆) δ ppm: 7.32 (s, 2H, -NH₂), 8.12 (s, 1H, -NH pyrimidine), 3.8 (s, 3H, -OCH₃), 6.14 (m, 2H, pyridine)
¹³C NMR (300 MHz, CDCl₃) δ ppm: 162.4, 160.2, 154.8, 152.6, 145.5, 118.2, 64.5.

2.2. Corrosion tests

2.2.1. Weight loss method

Weight loss measurements were performed at different temperatures (303–333 K). The accurately weighed mild steel test coupons were immersed for 6 h in 250 mL of 15% HCl solution in the absence and presence of 50, 100, 150 and 200 ppm (mgL^{-1}) of the inhibitors. The test coupons were then removed from the 15% HCl solution, washed thoroughly with distilled water, dried and weighed. Triplicate experiments were conducted for each concentration and temperature of the inhibitor for the reproducibility and the average of weight losses were taken to calculate different corrosion parameters. The corrosion rate (CR), inhibition efficiency ($\eta\%$) and surface coverage (θ) were determined by the following equations [20–22]:

$$CR(\text{mmy}^{-1}) = \frac{8.76 \times 10^4 \times W}{D \times A \times t} \quad (1)$$

where, W = weight loss (g), A = area of specimen (cm^2) exposed in solution, t = exposure time (h), and D = density of mild steel (g cm^{-3}).

$$\theta = \frac{CR_0 - CR_i}{CR_0} \quad (2)$$

$$\eta(\%) = \frac{CR_0 - CR_i}{CR_0} \times 100 \quad (3)$$

where, CR_0 and CR_i are corrosion rate in absence and presence of inhibitors.

2.2.2. Electrochemical studies

The electrochemical studies were conducted in a conventional three-electrode cell consisting of mild steel sample of 1 cm^2 exposed area as working electrode, a platinum counter electrode and a saturated calomel electrode (SCE) as reference electrode, using CH electrochemical workstation (Model No: CHI 760D, manufactured by CH Instruments, Austin, USA) at 303 K. Before impedance and polarization measurements, the working electrode was immersed in the test solution until a steady-state of the open-circuit potential corresponding to the corrosion potential (E_{corr}) of the working electrode was obtained. Potentiodynamic polarization curves were obtained by changing the electrode potential from -200 to $+200$ mV vs SCE at OCP at a scan rate of 1 mVs^{-1} . The linear Tafel segments of anodic and cathodic curves were extrapolated to obtain corrosion current densities (i_{corr}).

EIS measurements were carried out using AC signals of amplitude 10 mV peak to peak at the open circuit potential in the frequency

range 100 kHz to 10 mHz. All impedance data were fitted to appropriate circuits using ZSimpWin.3.21 software.

2.2.3. Scanning electron microscopic and energy dispersive spectroscopy analysis

The mild steel specimens of size $1.0 \text{ cm} \times 1.0 \text{ cm} \times 0.1 \text{ cm}$ were abraded with a series of emery paper (grade 320–500–800–1200) and then washed with distilled water and acetone. After 6 h immersion of the specimen in 15% HCl solution in the absence and the presence of optimum concentration (200 ppm) of inhibitors (MPPA and AMPO) at 303 K, the specimen was taken out, cleaned with distilled water, dried with a cold air blaster, and then the SEM and EDX images were recorded using the instrument HITACHI S3400N.

2.2.4. Atomic force microscopy (AFM)

The morphology of the polished, uninhibited and inhibited mild steel surface was investigated by AFM. For AFM analysis the mild steel specimens of size $1 \text{ cm} \times 1 \text{ cm} \times 0.1 \text{ cm}$ were immersed in the test solution for 6 h in the absence and presence of inhibitors at 303 K. Then the specimens were taken out from the solution, cleaned with distilled water, dried, and used for AFM images. The AFM analyses were carried out using a Nanosurf Easyscan2 instrument, Model: NT-MDT, Russia; Solver Pro-47.

2.2.5. Quantum chemical study

Complete geometrical optimizations of the investigated molecules were performed using density functional theory (DFT) in aqueous phase with the Becke's three parameter exchange functional along with the Lee–Yang–Parr nonlocal correlation functional (B3LYP) with 6-31G (d, p) basis set as implemented in Gaussian 03 program package [29]. Theoretical parameters such as the energies of the highest occupied and lowest unoccupied molecular orbital (E_{HOMO} and E_{LUMO}), energy gap (ΔE) and dipole moment (μ) were determined.

3. Results and discussion

3.1. Weight loss measurements

3.1.1. Effect of inhibitor concentration and temperature

The corrosion parameters such as corrosion rate (CR), surface coverage (θ) and corrosion inhibition efficiency ($\eta\%$) obtained by weight loss measurements for mild steel specimen immersed in 15% HCl solution in the absence and presence of different concentration ranges of (50–200 ppm) of inhibitors (MPPA, AMPO) for an immersion period of 6 h at different temperature ranges of (303–333) K and are listed in Table 1. From Table 1, it is apparent that inhibition efficiency increased with increasing concentration of the inhibitors. By increasing the inhibitor concentration, the part of metal surface covered by inhibitor molecules increases and that leads to an increase in the inhibition efficiencies [30].

Both the inhibitors are good inhibitors even at the concentration as low as 50 ppm. The inhibition efficiency of MPPA and AMPO at

Table 1
Corrosion parameters namely corrosion rate (CR), surface coverage (θ) and inhibition efficiency ($\eta\%$) of mild steel in 15% HCl solution in the presence and absence of inhibitor at different temperature, obtained from weight loss measurements.

| Conc. (ppm) | 303 K | | | 313 K | | | 323 K | | | 333 K | | |
|-------------|-------------------------|----------|----------|-------------------------|----------|----------|-------------------------|----------|----------|-------------------------|----------|----------|
| | CR (mmy ⁻¹) | θ | $\eta\%$ | CR (mmy ⁻¹) | θ | $\eta\%$ | CR (mmy ⁻¹) | θ | $\eta\%$ | CR (mmy ⁻¹) | θ | $\eta\%$ |
| Blank | 28.2 | – | – | 58.1 | – | – | 98.9 | – | – | 144.5 | – | – |
| <i>AMPO</i> | | | | | | | | | | | | |
| 50 | 3.76 | 0.86 | 86.6 | 8.88 | 0.83 | 84.7 | 16.51 | 0.81 | 83.3 | 26.15 | 0.81 | 81.9 |
| 100 | 2.56 | 0.90 | 90.9 | 6.62 | 0.87 | 88.6 | 12.16 | 0.85 | 87.7 | 20.08 | 0.84 | 86.1 |
| 150 | 1.72 | 0.93 | 93.9 | 4.88 | 0.91 | 91.6 | 9.29 | 0.90 | 90.6 | 15.46 | 0.91 | 89.3 |
| 200 | 0.87 | 0.96 | 96.9 | 3.13 | 0.94 | 94.6 | 6.13 | 0.93 | 93.8 | 10.98 | 0.93 | 92.4 |
| <i>MPPA</i> | | | | | | | | | | | | |
| 50 | 3.58 | 0.87 | 87.3 | 8.71 | 0.85 | 85.0 | 15.72 | 0.84 | 84.1 | 24.42 | 0.83 | 83.1 |
| 100 | 2.39 | 0.91 | 91.5 | 6.21 | 0.89 | 89.3 | 11.67 | 0.88 | 88.2 | 18.49 | 0.87 | 87.2 |
| 150 | 1.55 | 0.94 | 94.5 | 4.47 | 0.92 | 92.3 | 8.60 | 0.91 | 91.3 | 14.16 | 0.90 | 90.2 |
| 200 | 0.62 | 0.97 | 97.8 | 2.55 | 0.95 | 95.6 | 5.43 | 0.94 | 94.5 | 9.24 | 0.93 | 93.6 |

Experimental errors \pm 3%.

200 ppm concentration was found to be 97.8% and 96.9% respectively, while it was 87.3% and 86.6% respectively, at 50 ppm concentration at 303 K (Table 1). The inhibition efficiency of both the inhibitors decreased with increasing temperature from 303 to 333 K (Table 1). This is due to the fact that at higher temperatures the metal dissolution process is enhanced and the adsorbed inhibitor molecules are partially desorbed from the metal surface [31].

3.1.2. Thermodynamic and activation parameters

The apparent activation energy (E_a) for dissolution of mild steel in 15% HCl solution was calculated by using Arrhenius equation:

$$\log CR = \frac{-E_a}{2.303RT} + \log A \quad (4)$$

where R is the molar gas constant ($8.314 \text{ J K}^{-1} \text{ mol}^{-1}$), T is the absolute temperature (K) and A is the Arrhenius pre-exponential factor. Fig. 2 presents the Arrhenius plot of $\log CR$ against $1/T$ for the corrosion of mild steel in 15% HCl solution in the absence and presence of inhibitors at concentrations ranging from 50 to 200 ppm. From the slope in Fig. 2, the values of E_a were calculated and summarized in Table 2. It is evident from Table 2 that the values of the apparent activation energy for the inhibited solutions were higher than that for the uninhibited solution, indicating that the dissolution of mild steel was decreased due to formation of a barrier by the adsorption of the inhibitors on metal surface [32].

The values of standard enthalpy of activation (ΔH^*) and standard entropy of activation (ΔS^*) were calculated by using the transition state equation

$$CR = \frac{RT}{Nh} \exp\left(\frac{\Delta S^*}{R}\right) \exp\left(-\frac{\Delta H^*}{RT}\right) \quad (5)$$

where, h is the Planck's constant and N is the Avogadro number, respectively.

A plot of $\log (CR/T)$ against $1/T$ (Fig. 3) gave straight lines with a slope of $-\Delta H^*/2.303R$ and an intercept of $[\log(R/Nh) + (\Delta S^*/2.303R)]$, from which the activation thermodynamic parameters (ΔH^* and ΔS^*) were calculated, and are listed in Table 2. The negative value of ΔS^* for both inhibitors indicates that the formation of the activated complex in the rate determining step represents an association rather than a dissociation step, meaning that a decrease in disorder takes place during the course of the transition from reactants to activated complex [33].

3.1.3. Adsorption isotherm

The plots of C_{inh}/θ vs. C_{inh} yielded straight lines (Fig. 4) with correlation coefficient (R^2) and slope values given in Table 3 at studied temperatures. The correlation coefficient and slope values in Table 3 are near

unity indicating that the adsorption of both the inhibitors obeys Langmuir adsorption isotherm represented by the following equation:

$$\frac{C_{\text{inh}}}{\theta} = \frac{1}{K_{\text{ads}}} + C_{\text{inh}} \quad (6)$$

where C_{inh} is the inhibitor concentration, K_{ads} is the equilibrium constant for adsorption–desorption process.

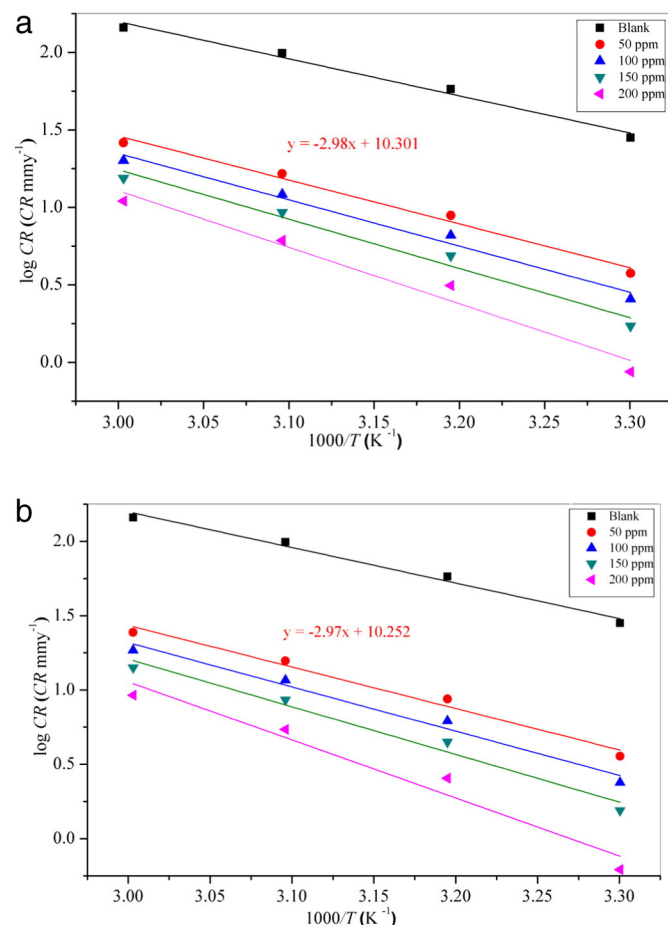


Fig. 2. Arrhenius plots of $\log CR$ versus $1000/T$ for mild steel corrosion in 15% HCl solution (a) AMPO (b) MPPA.

Table 2

Activation parameters for mild steel in 15% HCl solution in the absence and presence of inhibitor obtained from weight loss measurements.

| Inhibitor | Concentration (ppm) | E_a (kJmol ⁻¹) | ΔH^* (kJ mol ⁻¹) | ΔS^* (Jmol ⁻¹ K ⁻¹) |
|-----------|---------------------|------------------------------|--------------------------------------|--|
| Blank | – | 45.7 | 43.0 | –74.4 |
| AMPO | 50 | 53.1 | 51.5 | –63.2 |
| | 100 | 55.3 | 54.2 | –56.5 |
| | 150 | 57.9 | 58.2 | –47.2 |
| | 200 | 61.8 | 67.0 | –38.6 |
| MPPA | 50 | 55.0 | 58.7 | –54.4 |
| | 100 | 60.5 | 71.9 | –46.3 |
| | 150 | 63.5 | 43.0 | –44.7 |
| | 200 | 71.0 | 50.7 | –65.8 |

Experimental errors ± 3%.

The values of K_{ads} were calculated from the intercept of Fig. 4. Large values of K_{ads} were obtained for both studied inhibitors suggesting more efficient adsorption and hence better corrosion inhibition efficiency. Using the values of K_{ads} , the values of ΔG_{ads} were obtained by using the following equation:

$$\Delta G_{ads}^0 = -RT \ln(55.5K_{ads}) \quad (7)$$

The value of 55.5 is the concentration of water in solution in mol L⁻¹.

The calculated values of K_{ads} and ΔG_{ads} are listed in Table 3. In general, values of ΔG_{ads} up to –20 kJmol⁻¹ are compatible with physisorption and those which are more negative than –40 kJmol⁻¹ involve chemisorptions [34]. The calculated ΔG_{ads} values for AMPO

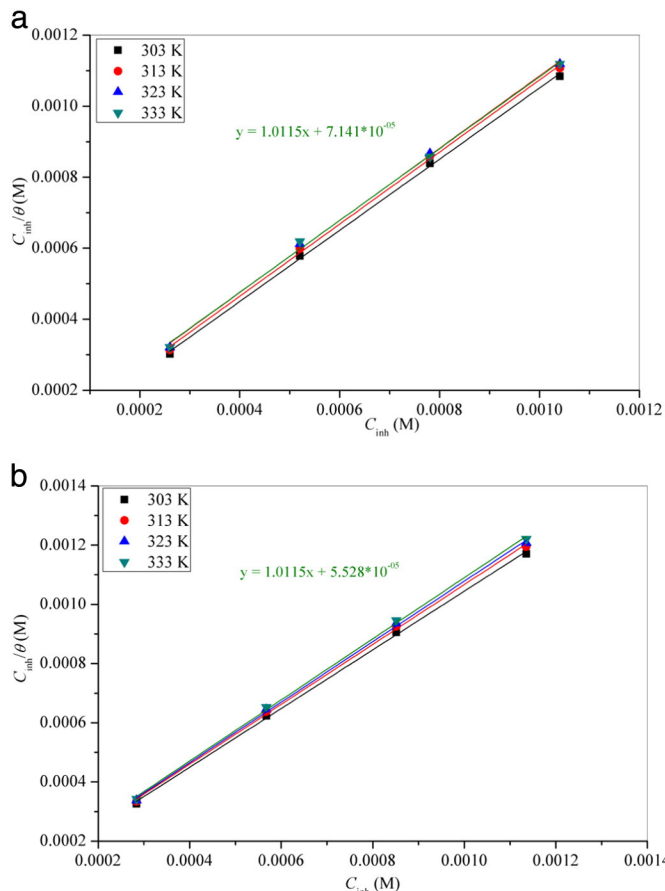


Fig. 4. Langmuir plots of (C_{inh}/θ) versus C_{inh} for (a) AMPO (b) MPPA.

and MPPA were found in the range of –35.0 to –37.5 and –36.7 to –38.2 kJmol⁻¹, respectively, at different temperatures (303–333) K, these values were between the threshold values for physical adsorption and chemical adsorption, indicating that the adsorption process of inhibitors at mild steel surface involve both the physical as well as the chemical adsorption.

4. Electrochemical studies

4.1. Polarization studies

The potentiodynamic polarization curves for the mild steel in 15% HCl solution in the absence and presence of different concentrations of AMPO and MPPA at 303 K and are shown in Fig. 5a, b. The corrosion parameters such as corrosion potential (E_{corr}), anodic Tafel slope (β_a),

Table 3

Adsorption parameters for AMPO and MPPA calculated from Langmuir adsorption isotherm for mild steel in 15% HCl solution at temperature range of 303–333 K.

| Inhibitor | Temperature (K) | K_{ads} (M ⁻¹) | ΔG_{ads}^0 (kJ mol ⁻¹) | Correlation coefficient (R^2) | Slope values |
|-----------|-----------------|------------------------------|--|-----------------------------------|--------------|
| AMPO | 303 | 2.02×10^4 | –35.0 | 0.9989 | 1.001 |
| | 313 | 1.69×10^4 | –35.7 | 0.9986 | 1.014 |
| | 323 | 1.47×10^4 | –36.5 | 0.9981 | 1.018 |
| | 333 | 1.40×10^4 | –37.5 | 0.9970 | 1.011 |
| MPPA | 303 | 1.76×10^4 | –36.7 | 0.9989 | 1.021 |
| | 313 | 1.72×10^4 | –36.8 | 0.9988 | 1.032 |
| | 323 | 1.88×10^4 | –37.2 | 0.9989 | 0.991 |
| | 333 | 1.80×10^4 | –38.2 | 0.9989 | 1.011 |

Experimental errors ± 3%.

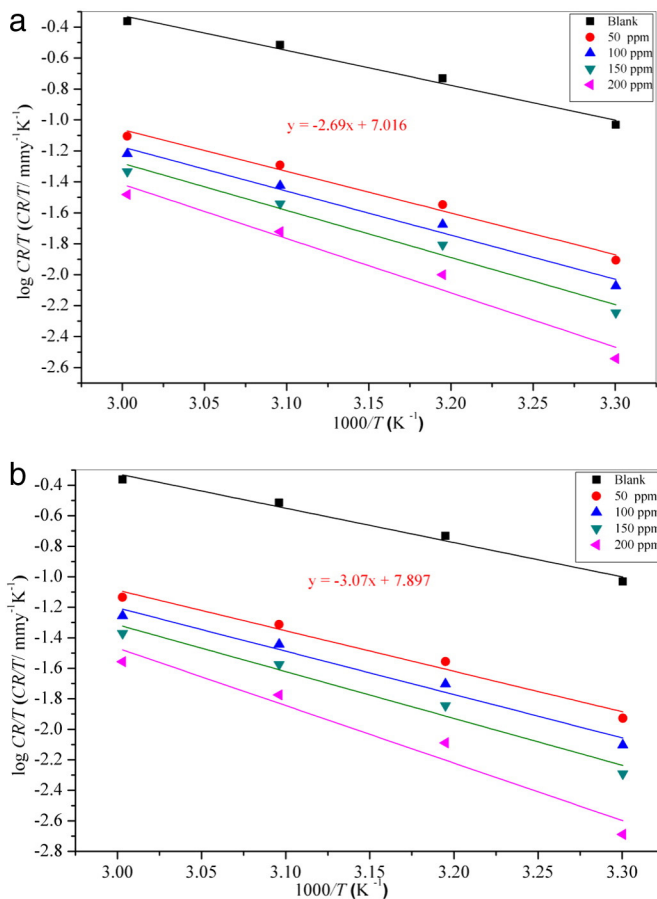


Fig. 3. Transition state plot of $\log CR/T$ versus $1000/T$ for mild steel in 15% HCl solution at different concentration (a) AMPO (b) MPPA.

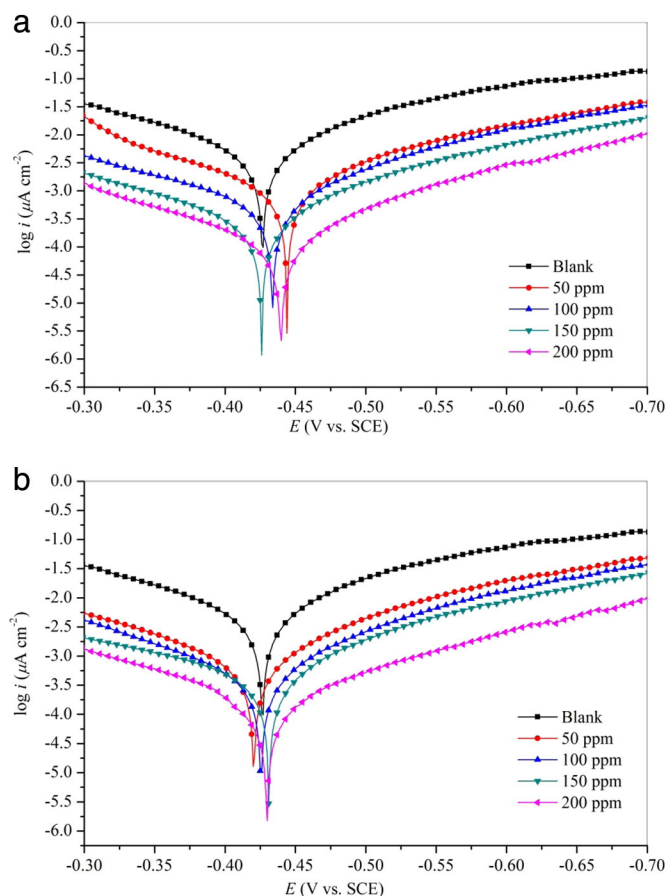


Fig. 5. Potentiodynamic polarization curves for mild steel in 15% HCl solution in the presence and absence of inhibitor 303 K (a) AMPO (b) MPPA.

cathodic Tafel slope (β_c) and corrosion current density (i_{corr}) obtained from these curves are given in Table 4. The percentage inhibition efficiency (η %) was calculated using the equation

$$\eta(\%) = \frac{i_{\text{corr}}^0 - i_{\text{corr}}}{i_{\text{corr}}^0} \times 100 \quad (8)$$

where, i_{corr}^0 and i_{corr} are the values of corrosion current density in the absence and presence of inhibitors, respectively.

It is apparent in Fig. 5, that both anodic metal dissolution of iron and cathodic hydrogen evolution curves shifted towards lower current density after the addition of inhibitors to 15% HCl solution. The lower corrosion current density (i_{corr}) values in the presence of inhibitor suggesting that the inhibitor molecules adsorbed on the surface of mild steel,

Table 4

Electrochemical parameter and percentage inhibition efficiency (H %) obtained from polarization studies for mild steel in 15% HCl solution in the absence and presence of inhibitor at 303 K.

| Inhibitor | Conc. (ppm) | $-E_{\text{corr}}$ (mV/SCE) | i_{corr} ($\mu\text{A cm}^{-2}$) | β_a (mV dec^{-1}) | β_c (mV dec^{-1}) | θ | η (%) |
|-----------|-------------|-----------------------------|---|------------------------------------|------------------------------------|----------|------------|
| Blank | 0 | 416 | 6733 | 332 | 338 | – | – |
| AMPO | 50 | 415 | 862 | 277 | 339 | 0.87 | 87.2 |
| | 100 | 438 | 586 | 357 | 286 | 0.91 | 91.3 |
| | 150 | 420 | 397 | 324 | 291 | 0.94 | 94.1 |
| | 200 | 446 | 175 | 319 | 271 | 0.97 | 97.4 |
| MPPA | 50 | 422 | 821 | 319 | 283 | 0.87 | 87.8 |
| | 100 | 422 | 539 | 278 | 269 | 0.92 | 92.0 |
| | 150 | 445 | 323 | 370 | 285 | 0.95 | 95.2 |
| | 200 | 462 | 128 | 339 | 306 | 0.98 | 98.1 |

Experimental errors $\pm 1\%$.

thereby blocking the corrosion reaction [35] and increasing the inhibition efficiency. The anodic Tafel slope (β_a) and the cathodic Tafel slope (β_c) of AMPO and MPPA changed with inhibitor concentration, indicating that these inhibitors controlled both anodic as well as cathodic reactions and act as mixed inhibitor.

The presence of inhibitor caused minor change in E_{corr} values with respect to the E_{corr} value in the absence of inhibitor. It was reported by various researchers that if the change in E_{corr} value in the presence of inhibitor is more than 85 mV, the inhibitor is recognized as an anodic or a cathodic type inhibitor whereas if the change in E_{corr} value is less than 85 mV, the inhibitor is recognized as mixed type inhibitor [36]. In the present investigation the maximum shift in E_{corr} was 46 mV towards the cathodic direction indicating that the inhibitors AMPO and MPPA act as mixed type inhibitor with predominately cathodic effect.

4.2. EIS studies

The Nyquist plots for mild steel obtained at mild steel/15% HCl solution interface with and without the different concentrations of AMPO and MPPA at 303 K and are shown in Fig. 6. The existence of a depressed semicircle with its centre below the axis (Z) in Nyquist plots (Fig. 6 a, b) for both inhibitors is suggesting the non-homogeneity and roughness of the mild steel surface [37]. The EIS spectra of all tests were analyzed using the equivalent circuit shown in Fig. 7, which is a parallel combination of the charge transfer resistance (R_{ct}) and the constant phase element (CPE), both in series with the solution resistance (R_s). This type of electrochemical equivalent circuit was reported previously to model

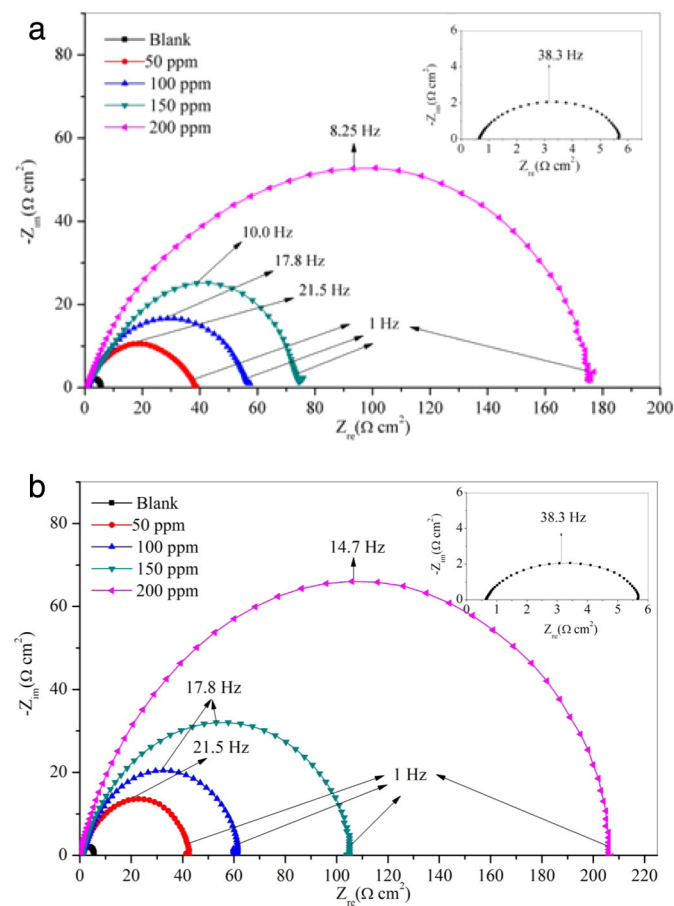


Fig. 6. Nyquist plots for mild steel in 15% HCl solution (a) AMPO (b) MPPA containing various concentrations (1) 0 ppm (2) 50 ppm (3) 100 ppm (4) 150 ppm (5) 200 ppm at 303 K.

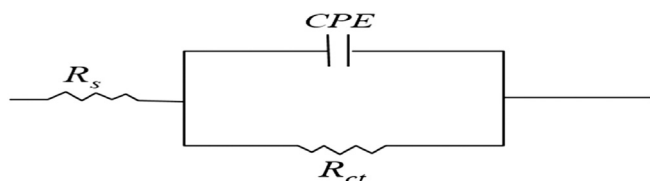


Fig. 7. Equivalent circuit diagram of a protective layer on the electrode surface.

Table 5

Electrochemical impedance parameters for mild steel in 15% HCl solution in the absence and presence of inhibitor at different concentration at 303 K.

| Inhibitor | Conc. (ppm) | R_s ($\Omega \text{ cm}^2$) | R_{ct} ($\Omega \text{ cm}^2$) | Y_0 ($\mu\text{F cm}^{-2}$) | n | C_{dl} ($\mu\text{F cm}^{-2}$) | $\eta\%$ |
|-----------|-------------|---------------------------------|------------------------------------|---------------------------------|------|------------------------------------|----------|
| Blank | – | 0.65 | 5.1 | 1471 | 0.87 | 721.1 | – |
| AMPO | 50 | 0.85 | 37.4 | 981 | 0.70 | 250.0 | 86.3 |
| | 100 | 0.89 | 57.0 | 730 | 0.71 | 199.5 | 91.0 |
| | 150 | 0.82 | 78.9 | 510 | 0.72 | 146.6 | 93.5 |
| | 200 | 0.82 | 171.8 | 218 | 0.77 | 82.7 | 97.0 |
| MPPA | 50 | 0.86 | 41.7 | 803 | 0.72 | 214.7 | 87.7 |
| | 100 | 0.85 | 63.5 | 487 | 0.74 | 145.9 | 92.0 |
| | 150 | 0.82 | 105.4 | 278 | 0.76 | 93.3 | 95.1 |
| | 200 | 0.27 | 209.8 | 114 | 0.80 | 44.8 | 97.6 |

Experimental errors $\pm 1\%$.

the iron/acid interface [38]. CPE is introduced instead of pure double layer capacitance to give more accurate fit as the double layer at interface does not behave as ideal capacitor.

The electrochemical parameters such as solution resistance, charge transfer resistance and CPE constants (Y_0 and n) obtained from fitting

the experimental data of Nyquist plots in the equivalent circuit shown in Fig. 7 are presented in Table 5.

The inhibition efficiency ($\eta\%$) was calculated from charge transfer resistance values obtained from impedance measurements using the following relation

$$\eta(\%) = \frac{R_{ct(\text{inh})} - R_{ct}}{R_{ct(\text{inh})}} \times 100 \quad (9)$$

where $R_{ct(\text{inh})}$ and R_{ct} are charge transfer resistance in the presence and absence of inhibitor respectively.

The values of double layer capacitance (C_{dl}) were calculated from charge transfer resistance and CPE parameters (Y_0 and n) using the expression [39]

$$C_{dl} = (Y_0 R_{ct}^{1-n})^{1/n} \quad (10)$$

where Y_0 is the CPE constant and n is the CPE exponent. The value of n represents the deviation from the ideal behavior and it lies between 0 and 1.

The results showed that the charge transfer resistance for blank solution was relatively low due to high conductance of HCl solution. Similar value of R_{ct} for blank solution was also reported by other researchers [40]. The data shown in Table 5 reveal that the value of R_{ct} increases with addition of inhibitors as compared to the blank solution, the increase in R_{ct} value is attributed to the formation of a protective film at the metal/solution interface. The C_{dl} value decreases on increasing the concentration of both the inhibitors, indicating the decrease in local dielectric constant and/or to an increase in the thickness of the electrical

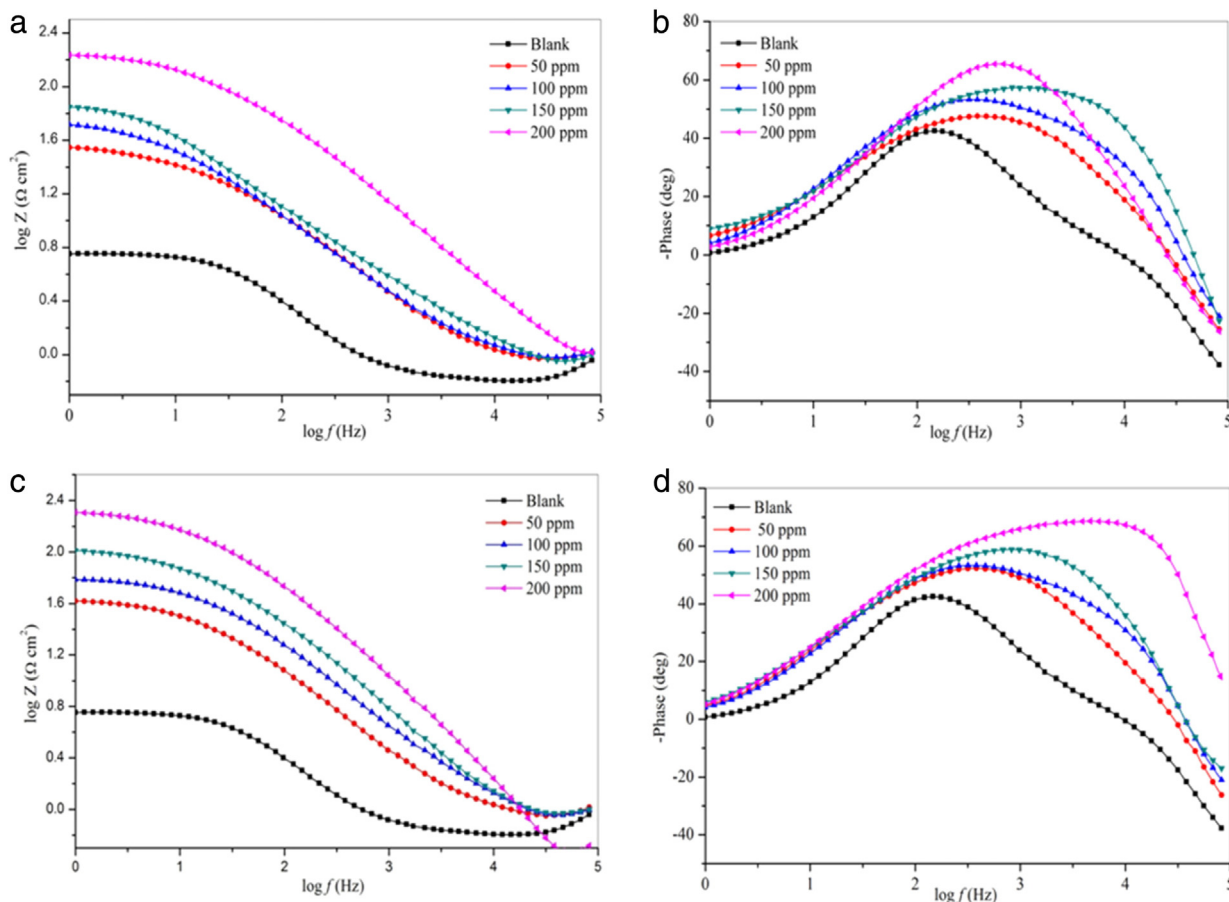


Fig. 8. Bode plots for mild steel in a 15% HCl solution in the absence and presence of different concentrations of inhibitors (a) AMPO (b) MPPA.

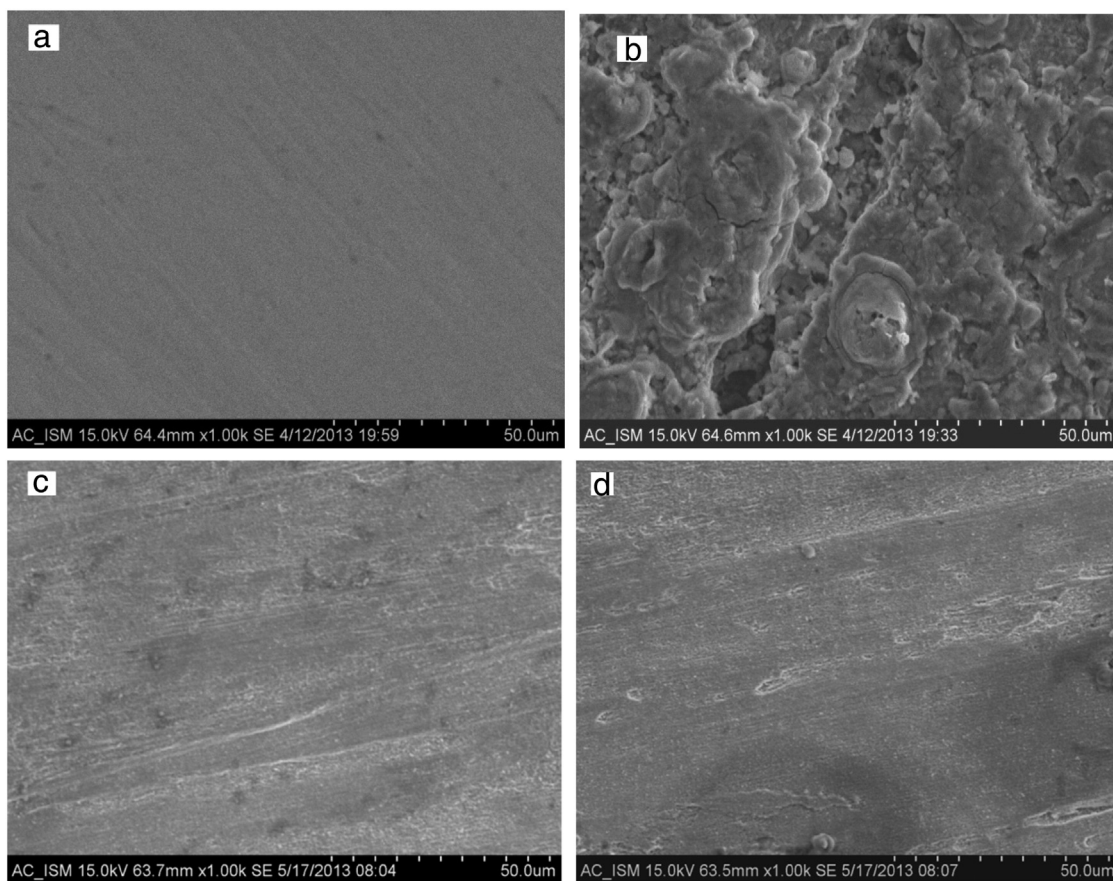


Fig. 9. SEM image of mild steel in 15% HCl solution after 6 h immersion at 303 K (a) before immersion (polished), (b) after immersion without inhibitor, (c) with inhibitor MPPA, (d) with inhibitor AMPO.

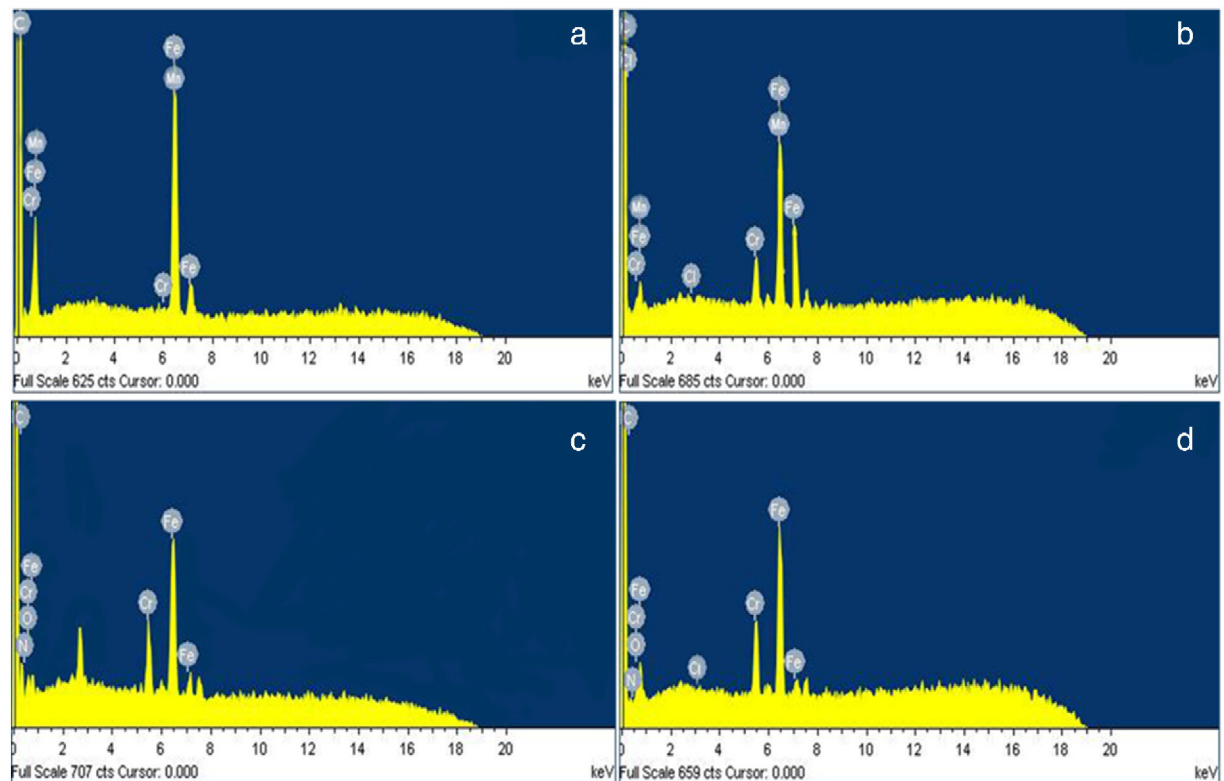


Fig. 10. EDX spectra of mild steel specimens (a) polished, (b) after immersion without inhibitor, (c) with 200 ppm AMPO, (d) with 200 ppm MPPA.

Table 6

Percentage atomic contents of elements obtained from EDX spectra.

| Inhibitors | Fe | C | Cr | Mn | Cl | N | O |
|-------------------------|-------|-------|------|------|------|------|-------|
| Polished mild steel | 85.26 | 12.46 | 0.86 | 0.46 | – | – | – |
| Mild steel in blank HCl | 83.12 | 15.68 | 0.67 | 0.28 | 2.29 | – | 6.36 |
| Mild steel in AMPO | 68.12 | 17.36 | 0.58 | – | 0.35 | 3.65 | 8.46 |
| Mild steel in MPPA | 62.25 | 17.72 | 0.57 | – | 0.33 | 4.16 | 11.64 |

double layer, suggesting that the inhibitor molecules are adsorbed at the metal/solution interface.

The Bode phase angle plots (Fig. 8b, d) shows single maximum (one time constant) at intermediate frequencies, broadening of this maximum in the presence of inhibitors accounts for the formation of a protective layer on the electrode surface. Fig. 8a, c shows that the impedance value in the presence of both inhibitors is larger than in the absence of inhibitors and the value of impedance increases on increasing the concentration of both studied inhibitors. These mean that the corrosion rate is reduced in the presence of the inhibitors and continued to decrease on increasing the concentration of inhibitors.

Electrochemical results (η) are in good agreement with the results (η) obtained by weight loss experiment.

5. Scanning electron microscopy

SEM photomicrographs for mild steel in 15% HCl solution in the absence and presence of 200 ppm of AMPO and MPPA are shown in

Fig. 9a–d. The surface of the polished mild steel specimen (Fig. 9a) is very smooth and shows no corrosion while mild steel specimen dipped in 15% HCl solution in the absence of inhibitor (Fig. 9b) is very rough and the surface is damaged due to metal dissolution. However, the presence of 200 ppm of inhibitor suppresses the rate of corrosion and surface damage has been diminished considerably (Fig. 9c, d) as compared to the blank solution (Fig. 9b) suggesting formation of a protective inhibitor film at the mild steel surface.

6. Energy dispersive spectroscopy

Energy dispersive X-ray analysis (EDX) technique was employed in order to get information about the composition of the surface of the mild steel sample in absence and presence of inhibitors in 15% HCl solution. The results of EDX spectra are shown in Fig. 10, a, b, c, d. The percentage atomic content of various elements of the polished, uninhibited and inhibited mild steel surface determined by EDX is shown in Table 6. The percentage atomic content of Fe for mild steel immersed in 15% HCl solution is 83.12%, and those for mild steel dipped in an optimum concentration (200 ppm) of AMPO, and MPPA are 68.12% and 62.25%, respectively. In Fig. 10, the spectra of inhibited samples show that the Fe peaks are considerably suppressed, when compared with the polished and uninhibited mild steel sample. This suppression of Fe lines is due to the inhibitory film formed on the mild steel surface. The EDX spectra of inhibited mild steel contain the peaks corresponding to all the elements present in the inhibitor molecules indicating the adsorption of inhibitor molecules at the surface of mild steel.

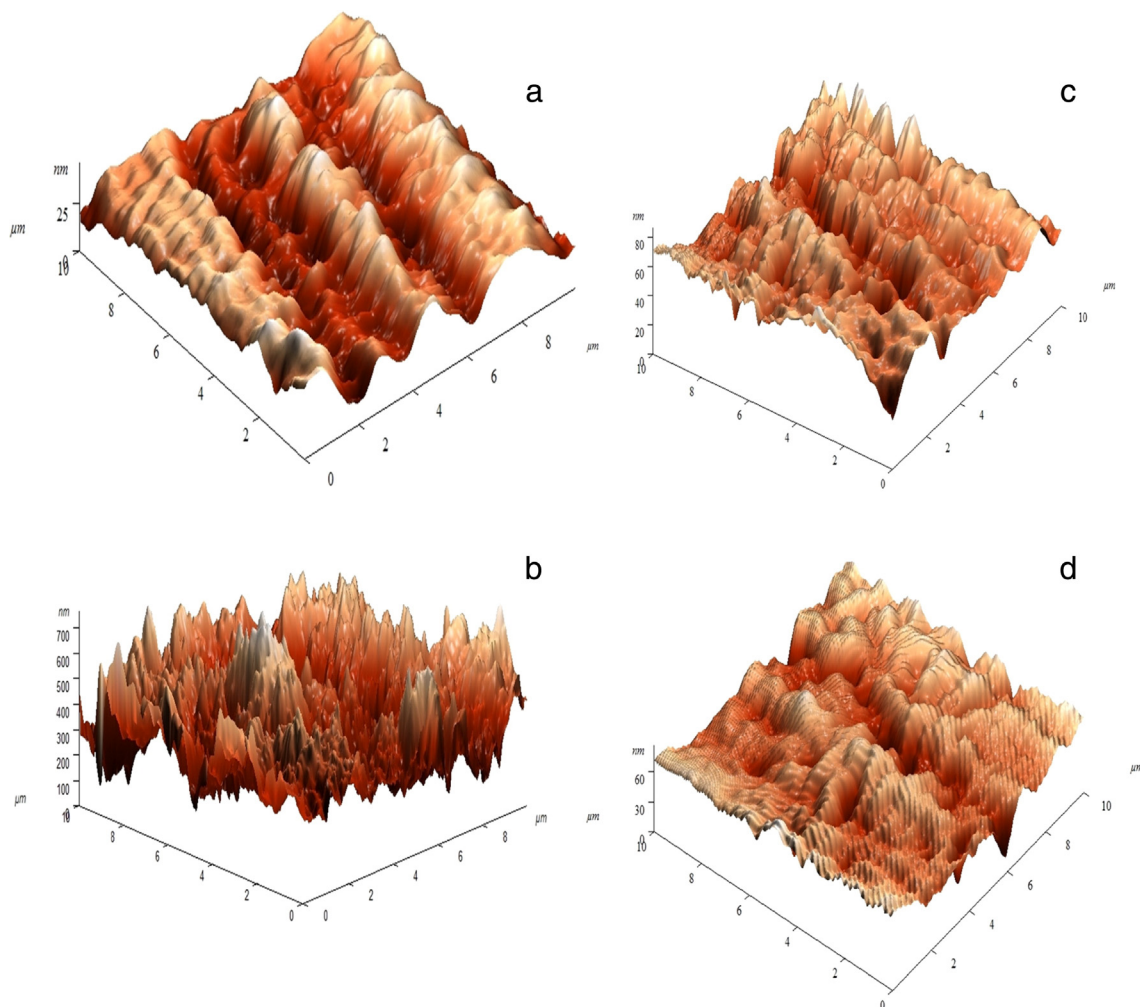


Fig. 11. Atomic force micrographs of mild steel surface (a) polished mild steel, (b) mild steel in 15% HCl solution, and (c) in presence of inhibitor AMPO, (d) MPPA.

7. AFM

The three-dimensional AFM images of polished, uninhibited and inhibited mild steel samples are shown in Fig. 11a–d. The average roughness of polished mild steel sample (Fig. 11a) and mild steel sample in 15% HCl solution without inhibitor (Fig. 11b) were found as 25 and 650 nm. It is clearly shown in Fig. 11b that mild steel sample is badly damaged due to the acid attack on surface. However, in the presence of optimum concentration of 200 ppm of AMPO and MPPA as shown in Fig. 11c, d, the average roughness were reduced to 76 and 64 nm, respectively. The lower value of roughness for MPPA than AMPO reveals that MPPA protects the mild steel surface more efficiently than AMPO in 15% HCl solution.

8. Theoretical calculation

In order to study the effect of molecular structure on the inhibition efficiency, quantum chemical calculations were performed by using DFT and all the calculations were carried out with the help of complete geometry optimization. Optimized structures, E_{HOMO} and E_{LUMO} are shown in Fig. 12a, b. The quantum chemical parameters such as the energy of the highest occupied molecular orbital (E_{HOMO}), the energy of the lowest unoccupied molecular orbital (E_{LUMO}), energy gap (ΔE) and dipole moment (μ) were determined and summarized in Table 7. According to the frontier molecular orbital (FMO) theory of chemical reactivity, the formation of a transition state is due to interaction between HOMO and LUMO of reacting species. The smaller the orbital energy gap (ΔE) between the participating HOMO and LUMO, the stronger the interactions between two reacting species [41].

It was reported previously by some researchers that smaller values of ΔE and higher values of dipole moment (μ) are responsible for higher inhibition efficiency [42]. The lower values of the energy gap ΔE will render good inhibition efficiencies since the energy to remove an electron from the last occupied orbital will be minimized. According to HSAB theory hard acids prefer to co-ordinate to hard bases and soft acid to soft bases. Fe is considered as soft acid and will co-ordinate to molecule having maximum softness and small energy gap ($\Delta E = E_{\text{LUMO}} - E_{\text{HOMO}}$). Higher value of E_{HOMO} , μ and lower values of ΔE and

Table 7

Quantum chemical parameters for different inhibitors.

| Inhibitor | $-E_{\text{HOMO}}$ (eV) | $-E_{\text{LUMO}}$ (eV) | ΔE (eV) | μ (D) |
|-----------|-------------------------|-------------------------|-----------------|-----------|
| AMPO | 6.1630 | 1.2979 | 4.8715 | 4.396 |
| MPPA | 6.0515 | 1.4040 | 4.6475 | 4.565 |

E_{LUMO} for MPPA as compared to AMPO are indicating that MPPA has more potency to get adsorbed on the mild steel surface resulting in greater inhibition tendency than AMPO.

9. Mechanism of inhibition

Corrosion inhibition of mild steel in 15% hydrochloric acid solution by both inhibitors (MPPA and AMPO) can be explained on the basis of molecular adsorption. These compounds inhibit corrosion by controlling both anodic as well as cathodic reactions. In 15% hydrochloric acid solutions these inhibitors exist as protonated species. In both inhibitors the nitrogen atoms present in the molecules can be easily protonated in acidic solution and convert into quaternary compounds. These protonated species adsorbed on the cathodic sites of the mild steel and decrease the evolution of hydrogen. The adsorption on anodic site occurs through π -electrons of pyridine, and pyrimidine rings and lone pair of electrons of nitrogen atoms present in both the inhibitors which decrease the anodic dissolution of mild steel.

10. Conclusions

The synthesized pyrimidine derivatives act as good corrosion inhibitor for mild steel in 15% HCl solution and inhibiting performance of MPPA is better than AMPO. Polarization studies showed that both tested inhibitors are mixed type in nature. EIS measurements show that charge transfer resistance (R_{ct}) increases and double layer capacitance (C_{dl}) decreases in the presence of inhibitors, which suggested the adsorption of the inhibitor molecules on the surface of mild steel. The results obtained from SEM, EDX, AFM and Langmuir adsorption isotherm suggested that the mechanism of corrosion inhibition is occurring mainly through adsorption process. Quantum chemical results of AMPO and MPPA

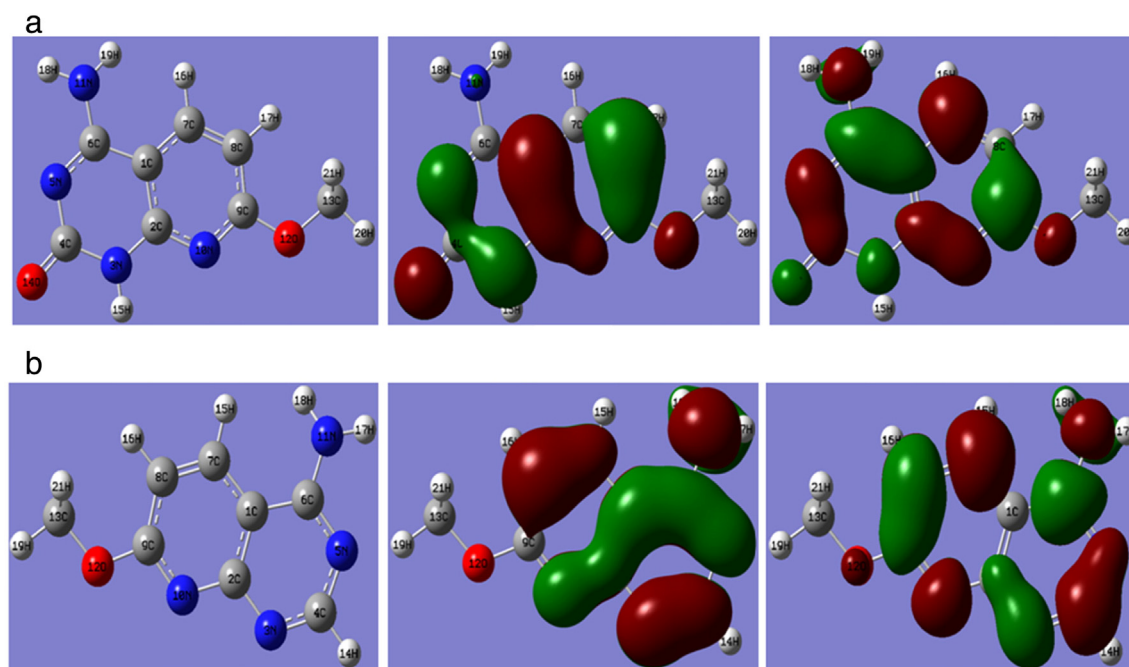


Fig. 12. The optimized structure (left) and HOMO (center) and LUMO (right) distribution for molecules (a) AMPO (b) MPPA [H, Gray; C, Cyan; N, Blue; O, Red]. (For interpretation of the references to color in this figure legend, the reader is referred to the web version of this article.)

showed higher value of E_{HOMO} , lower value of E_{LUMO} , and smaller value of ΔE , indicating that both inhibitors are good corrosion inhibitor for mild steel in 15% HCl solution.

Acknowledgments

The authors gratefully acknowledge the North-West University, Department of Science and Technology and the National Research Foundation (DST/NRF) South Africa grant funded (grant UID: 92333) for the postdoctoral scholarship of Dr I. Bahadur.

Appendix A. Supplementary data

Supplementary data to this article can be found online at <http://dx.doi.org/10.1016/j.molliq.2015.06.063>.

References

- [1] E.E. Ebenso, I.B. Obot, *Int. J. Electrochem. Sci.* 5 (2010) 2012–2035.
- [2] P. Mourya, P. Singh, A.K. Tewari, R.B. Rastogi, M.M. Singh, *Corros. Sci.* 95 (2015) 71–87.
- [3] G.E. Badr, *Corros. Sci.* 51 (2009) 2529–2536.
- [4] Y. Ren, Y. Luo, K. Zhang, G. Zhu, X. Tan, *Corros. Sci.* 50 (2008) 3147–3153.
- [5] K.S. Jacob, G. Parameswaran, *Corros. Sci.* 52 (2010) 224–228.
- [6] M.A. Amin, S.S. Abd El-Rehim, E.E.F. El-Sherbini, R.S. Bayoumi, *Electrochim. Acta* 52 (2007) 3588–3600.
- [7] D. Daoud, T. Douadi, H. Hamani, S. Chafaa, M. Al-Noaimi, *Corros. Sci.* 94 (2015) 21–37.
- [8] M.M. Antonijevic, G.D. Bogdanovic, M.B. Radovanovic, M.B. Petrovic, A.T. Stamenkovic, *Int. J. Electrochem. Sci.* 4 (2009) 654–661.
- [9] A. Zarrouk, B. Hammouti, T. Lakhlifi, M. Traisnel, H. Vezin, F. Bentiss, *Corros. Sci.* 90 (2015) 572–584.
- [10] X. Li, X. Xie, S. Deng, G. Du, *Corros. Sci.* 87 (2014) 27–39.
- [11] M.V. Fiori-Bimbi, P.E. Alvarez, H. Vaca, C.A. Gervasi, *Corros. Sci.* 92 (2015) 192–199.
- [12] H.M. Abd El-Lateef, *Corros. Sci.* 92 (2015) 104–117.
- [13] H. Hamani, T. Douadi, M. Al-Noaimi, S. Issaadi, D. Daoud, S. Chafaa, *Corros. Sci.* 88 (2014) 234–245.
- [14] R.D. Goyal, L. Prakash, *Indian J. Chem.* 31B (1992) 719.
- [15] A. Rahamana, H.N. Hafez, *Bioorg. Med. Chem.* 19 (2009) 3392–3397.
- [16] H. Huang, D.A. Hutta, R.L. Desfarlais, C. Schuberh, L.P. Ptronnia, M.A. Chaikin, C. Manthey, M.R. Player, *Bioorg. Med. Chem. Lett.* 18 (2008) 2355–2361.
- [17] G.Y. Elewady, *Int. J. Electrochem. Sci.* 3 (2008) 1149–1161.
- [18] N. Caliskan, E. Akbas, *Mater. Corros.* 63 (2012) 231–237.
- [19] X.H. Li, X.G. Xie, *Acta Phys.-Chim. Sin.* 29 (2013) 2221–2231.
- [20] M. Yadav, D. Behera, S. Kumar, R.R. Sinha, *Ind. Eng. Chem. Res.* 52 (2013) 6318–6328.
- [21] M. Yadav, D. Behera, U. Sharma, *Corros. Eng. Sci. Technol.* 48 (2013) 19–27.
- [22] M. Yadav, D. Behera, U. Sharma, *Arab. J. Chem.* (2012) <http://dx.doi.org/10.1016/j.arabjc.2012.03.011>.
- [23] H. Vashisht, S. Kumar, I. Bahadur, G. Singh, *Int. J. Electrochem. Sci.* 8 (2013) 684–699.
- [24] H. Vashisht, I. Bahadur, S. Kumar, K. Bhrara, D. Ramjugernath, G. Singh, *Int. J. Electrochem. Sci.* 9 (2014) 2896–2911.
- [25] H. Vashisht, I. Bahadur, S. Kumar, G. Singh, D. Ramjugernath, E.E. Ebenso, *Int. J. Electrochem. Sci.* 9 (2014) 5204–5221.
- [26] M. Yadav, S. Kumar, D. Behera, I. Bahadur, D. Ramjugernath, *Int. J. Electrochem. Sci.* 9 (2014) 5235–5257.
- [27] M. Yadav, S. Kumar, D. Behera, I. Bahadur, D. Ramjugernath, *Int. J. Electrochem. Sci.* 9 (2014) 3928–3950.
- [28] S. Bhargava, L.K. Rajwanshi, *Indian J. Chem.* 52B (2013) 448–452.
- [29] C. Lee, W. Yang, R.G. Parr, *Phys. Rev. B* 37 (1988) 785–789.
- [30] M.A. Hegazy, A.M. Badawi, S.S. Abd El Rehim, W.M. Kamel, *Corros. Sci.* 69 (2013) 110–122.
- [31] L. Fragoza-Mar, O. Olivares-Xometl, M.A. Domínguez-Aguilar, E.A. Flores, P. Arellanes-Lozada, F. Jimenez-Cruz, *Corros. Sci.* 61 (2012) 171–184.
- [32] I. Dehri, M. Ozcan, *Mater. Chem. Phys.* 98 (2006) 316–323.
- [33] X. Wang, H. Yang, F. Wang, *Corros. Sci.* 53 (2011) 113–121.
- [34] M. Behpour, S.M. Ghoreishi, N. Soltani, M. Salavati-Niasari, M. Hamadani, A. Gandomi, *Corros. Sci.* 50 (2008) 2172–2181.
- [35] M.S. Morad, A.M. Kamal El-Dean, *Corros. Sci.* 48 (2006) 3398–3412.
- [36] G.N. Mu, X.H. Li, Q. Qu, J. Zhou, *Corros. Sci.* 48 (2006) 445–459.
- [37] M. Lebrini, M. Lagrene'e, H. Vezin, M. Traisnel, F. Bentiss, *Corros. Sci.* 49 (2007) 2254–2269.
- [38] H. Gerengi, H.I. Sahin, *Ind. Eng. Chem. Res.* 51 (2012) 780–787.
- [39] M. Lebrini, F. Robert, A. Lecante, C. Roos, *Corros. Sci.* 53 (2011) 687–695.
- [40] P.B. Raja, A.K. Qureshi, A.A. Rahim, H. Osman, K. Awang, *Corros. Sci.* 69 (2013) 292–301.
- [41] S. Xia, M. Qiu, L. Yu, F. Liu, H. Zhao, *Corros. Sci.* 50 (2008) 2021–2029.
- [42] V.S. Sastri, J.R. Perumareddi, *Corrosion* 53 (1997) 617–622.